Journal of the Korean Astronomical Society
53: 35 ∼ 42, 2020 April
https://doi.org/10.5303/JKAS.2020.53.2.35
pISSN: 1225-4614 · eISSN: 2288-890X
http://jkas.kas.org

The Formation of the Double Gaussian Line Profiles of the Symbiotic Star AG Pegasi

Siek Hyung and Seong-Jae Lee

Department of Earth Science Education (Astronomy), Chungbuk National University, Chungbuk 28644, Korea
hyung@chungbuk.ac.kr, seong@chungbuk.ac.kr

Received December 12, 2019; accepted February 8, 2020

Abstract: We analyze high dispersion emission lines of the symbiotic nova AG Pegasi, observed in 1998, 2001, and 2002. The Hα and Hβ lines show three components, two narrow and one underlying broad line components, but most other lines, such as H I, He I, and He II lines, show two blue- and red-shifted components only. A recent study by Lee & Hyung (2018) suggested that the double Gaussian lines emitted from a bipolar conical shell are likely to form Raman scattering lines observed in 1998. In this study, we show that the bipolar cone with an opening angle of 74°, which expands at a velocity of 70 km s^{-1} along the polar axis of the white dwarf, can accommodate the observed double line profiles in 1998, 2001, and 2002. We conclude that the emission zone of the bipolar conical shell, which formed along the bipolar axis of the white dwarf due to the collimation by the accretion disk, is responsible for the double Gaussian profiles.

Key words: stars: binaries: symbiotic — stars: individual: AG Peg – ISM: dynamics and kinematics — ISM: lines and bands

1. Introduction

Symbiotic stars are identified as binary systems by their peculiar spectra, which show contributions by emission of both relatively low and very high temperature. However, it is difficult to confirm the presence of two stars in imaging studies. AG Pegasi was first reported as a Be star by Fleming (1907), after which Merrill (1916, 1942) observed He and Ca II absorption lines, numerous ionized or neutral emission lines, and TiO_2 absorption bands. Considered a Cyg-Be type star at the time of its discovery, AG Peg is now known as a symbiotic system composed of a Wolf-Rayet type white dwarf (WD) and a type M3 giant star (GS) (Merrill 1916; Hutchings et al. 1975). Spectroscopic monitoring of AG Peg has shown variations of its brightness and spectral intensities on time scales from months to decades. The orbital period is about 800 days. The temperature of the WD is about 100 000 K, while its cold component is a GS (Allen 1980; Viotti 1988; Nussbaumer 1992). Since the beginning of astronomical observations, two major outbursts have occurred: a first one in 1850, a second, shorter one in 2015.

In a symbiotic binary system, variations of emission line profiles might be caused by shielding effects partly due to the relative orientation of observer and binary system. Some earlier studies noted the presence of double Gaussian profiles or an absorption line at the center that might be associated with the GS passage at a specific phase (Contini 1997). However, the double Gaussian profiles seemed to exist at all phases and the GS cannot always be in front of the emission zone surrounding the WD. Lee & Hyung (2018), hereafter LH18, showed that a GS transit cannot form the observed Gaussian line profiles. Using spectroscopic data obtained at phases $\phi \sim 0.0$ or 0.5 with the Lick observatory, LH18 investigated whether the GS blocks the emission zone around the hot WD, causing the observed Gaussian line profiles. They provided some kinematic inference that the GS passages were not the source of the double Gaussian line profiles. Instead, LH18 demonstrated that a bipolar conical shell formed double Gaussian lines and that a broad line wing was formed by Raman scattering in the neutral region of the shell.

Raman scattering processes in symbiotic stars were proposed first by Schmid (1989), and Raman wings were first discussed by Nussbaumer et al. (1989) and further studied by Lee (2002). Lee & Hyung (2000) also showed that Raman scattering can occur in a dense planetary nebula such as IC 4997. Symbiotic stars have been considered as candidates for type Ia supernovae. The kinematic structure, including the physical conditions of the ionized hydrogen region and the symbiotic binary system, is of great interest. The mass inflow from the GS into the hot component might form an accretion disk. The fast stellar wind from the hot star is likely to develop bipolar conical shells that are responsible for both the double and broad emission lines. As the orbital phase, and thus the relative orientation of binary components and observer, changes, the shape of the line profiles changes accordingly. LH18 suggested that the bipolar conical shell is the most likely source of double Gaussian line profiles, but they did not compute theoretical line profiles for multiple phases. In this study, we fit the Hα or Hβ double Gaussian line profiles observed in arbitrary phases to a bipolar conical model.

Section 2 describes the observed spectra for three

Corresponding author: S.-J. Lee

Table 1
AG Peg observation log

Observation date (UT)	Julian Date	Phase (ϕ)
1998-09-17	2451073.70	10.24
2001-08-30	2452151.60	11.56
2002-08-11	2452498.92	11.98

epochs acquired by the Hamilton Echelle Spectrograph at Lick Observatory. Section 3 presents the predicted line profiles and the best parameters of a bipolar conical shell suitable for three epochs. We investigate the geometric structure of the system, responsible for the double Gaussian line profiles, observed in 1998, 2001, and 2002. Theoretical line profiles corresponding to different phases are provided to model the observed double line profiles. We conclude in Section 4.

2. LICK OBSERVATORY SPECTRAL DATA

Spectroscopic data were obtained by Lawrence H. Aller and Siek Hyung in 1998, 2001, and 2002 at the Lick observatory in the USA using the high-resolution Hamilton Echelle Spectrograph (HES) attached to the 3-meter Shane telescope. The spectral resolution of the HES is $R \sim 50\,000$. The slit width of the HES is 640 μm which corresponds to 1.2″ on the sky, the wavelength resolution is 0.1–0.2 Å/pixel. The observed spectral range is 3470–9775 Å, and we selected only the H and He lines from the various emission lines. Long exposure times of 1800 sec and 3600 sec were chosen for weak lines. Additional short-exposure spectra of 300 sec and 180 sec were obtained to avoid saturation of the strong Hα line. The IRAF standard star HR 7596 served as flux calibrator.

Table 1 shows the observation dates of AG Peg, Greenwich universal time (UT), Julian day, and phase. The phase of AG Peg is defined as zero when the WD is in front of the GS. The 2002 data (phase $\phi = 11.98$, 0.98 hereafter), close to $\phi = 0.0$, were secured when the WD was in front of the GS. The 2001 data (phase $\phi = 11.56$, 0.56 hereafter) is close to $\phi = 0.5$ when the GS was in front of the WD, i.e. when the GS could block the view onto the emission zone near the WD. In this study, we also used data from 1998 obtained at a phase $\phi = 10.24$ (0.24 hereafter) when WD and GS were close to their maximum separation on the sky. A detailed description of the 1998 spectral data is given in LH18.

The data were analyzed using the Image Reduction and Analysis Facilities (IRAF) software package of the National Optical Astronomy Observatory (NOAO). The spectra, with wavelengths in units of Å, were corrected for atmospheric extinction. We converted observed wavelengths to emitter frame wavelengths using the radial velocity of AG Peg relative to the Sun of -7.09 km s^{-1} which we obtained from a large number of permitted H I lines, namely the Balmer and the Paschen lines. Wavelengths were converted to speeds (in units of km s^{-1}) to make the kinematic characteristics visible directly. The final spectrum was further decomposed to find the kinematic subcomponents responsible for the full line profile, which involves a trial and error process that requires choosing the number of line components the observer can resolve. We used StarLink/Dipso provided by the Interactive Data Language (IDL) software and the European Southern Observatory (ESO) for this deconvolution.

Figure 1 shows the Hα lines observed in three epochs. To avoid saturation in the spectral line profiles, we used the 3 min and 5 min exposures. LH18 concluded that the Hα and Hβ hydrogen lines observed in 1998 are composed of three parts, a double line plus a broad wing, while the previous studies assumed four to five separate components with different kinematics, with suggested radial velocities being 60, 120, 400, and 1000 km s^{-1} (Kenyon et al. 1993; Eriksson et al. 2004). At first glance, only two line components are obvious. However, our detailed analysis (using IDL) separates the observed line profiles into three components. A detailed discussion of the three components is given in LH18 based on the 1998 data. The narrow double lines consist of blue- and red-shifted Gaussian components.

The Hα line observed in 1998 shows a red component that is substantially stronger than the blue one, while in 2001 the blue component is stronger than the red one. All observed line profiles in Figure 1 show the two narrow red-shifted and blue-shifted line components and one broad component. The full width at half maximum (FWHM) of the narrow lines is 60–120 km s^{-1} each, while the width of the broad line is 400–500 km s^{-1}. We adopted the kinematic center from the result of LH18 who analyzed the strong lines observed in 1998. One expects to see He II 6560 as well. Due to the relatively strong Hα emission, however, the He II 6560 line component(s) to the left of the Hα line cannot be resolved.

The Hβ line spectra shown in Figure 2 display two lines to the left of the Hβ components, corresponding to N III 4858 and He II 4559. Although the FWHMs of the Hβ line components are slightly different from those of the Hα spectral line profiles, both consist of three components.

We corrected the observed Hα and Hβ fluxes for interstellar extinction using a value of the extinction coefficient $C = \log I(\mathrm{H}\beta)/F(\mathrm{H}\beta) = 0.04$ (or color excess $E(B-V) = 0.027$) adopted from Kim & Hyung (2008) (hereafter KH08). The extinction-corrected ratio $I(\mathrm{H}\beta)/F(\mathrm{H}\beta)$ for the (blue plus red) flux is 2.87 for 1998, and those for 2001 and 2002 have similar values, 2.97 and 2.86, respectively. In 2001, the red components of both the Hα and Hβ lines are weak compared to the blue ones: the GS with its extended atmosphere may have blocked parts of the emission zone.

Inconsistencies in flux intensity or line width exist between the Hα and Hβ fluxes observed in 1998 and 2002. LH18 already noted their disagreement. Meanwhile, the Hα and Hβ fluxes observed in 2001 show a better agreement (see column 7 of Table 2). The discordance might partially be due to complex kinematics near the inner Lagrangian point and the GS with its extended atmosphere. When the GS blocks the view toward the

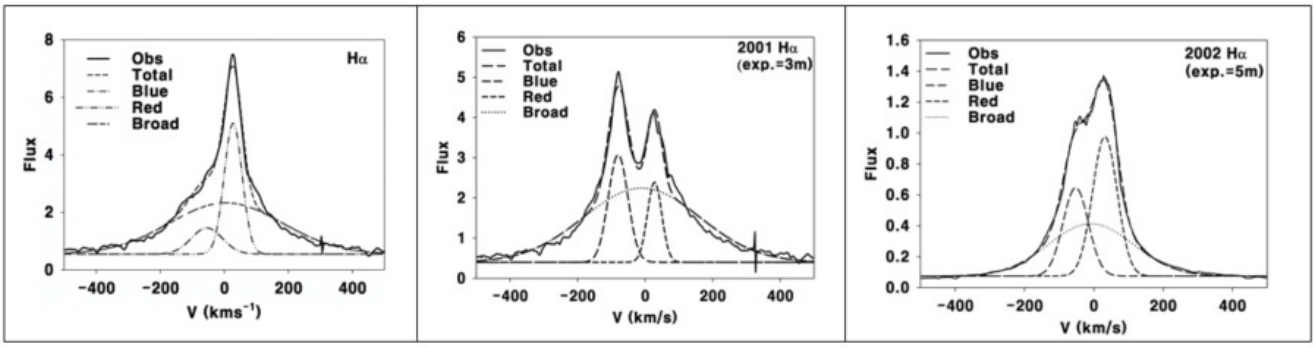

Figure 1. Hα spectral line profiles observed in 1998 (ϕ=0.24), 2001 (ϕ=0.56), and 2002 (ϕ=0.98), from left to right, respectively. Exposure times are 300 sec, 180 sec, and 300 sec, respectively. Radial velocities are given in units of km s^{-1}, fluxes in units of 10^{-11}erg s^{-1}cm^{-2} (per km s^{-1}). The kinematic center (location of 0 km s^{-1}) has been adapted from LH18.

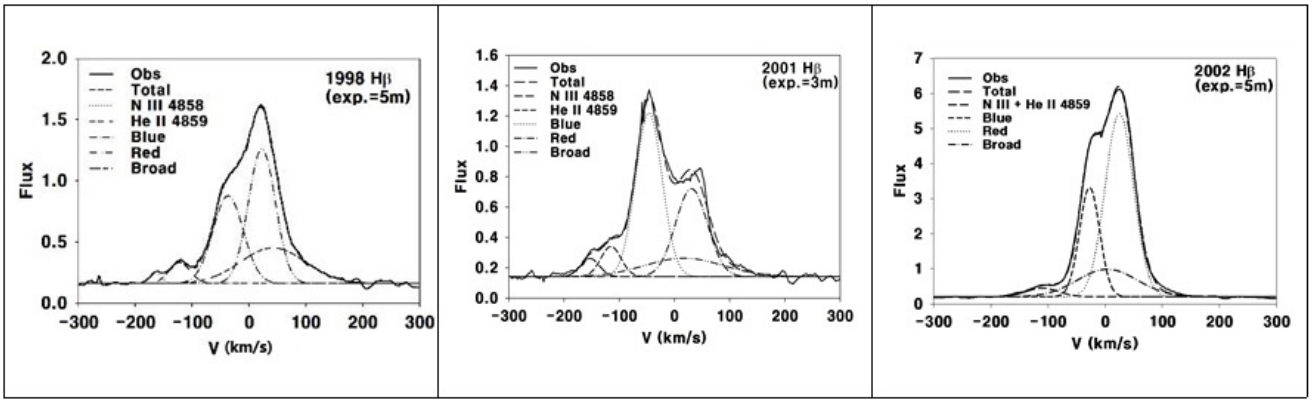

Figure 2. Like Figure 1 but for the Hβ spectral line profiles; see also LH18 for the 1998 Hβ line profile. The center of the broad line observed in 1998 is located at about 45 km s^{-1}, red-shifted from those in 2001 and 2002.

WD at $\phi \sim 0.5$, it also hides the inner Lagrangian point L1 and the extended atmosphere of the GS close to the WD. As a result, these regions are unlikely to contribute to the Hα and Hβ emission.

It is not straightforward to determine the kinematic center because three components are involved. However, the center of the broad line, which we assume to originate from Raman scattering, observed in 1998 seems to be about 45.0 km s^{-1} red-shifted relative to 2001 and 2002 (see Figure 2). If the emission zones are gravitationally bound to the WD, the kinematic center would be red-shifted at $\phi \sim 0.25$ relative to those at $\phi \sim 0.0$ or 0.5 (See Figure 4).

Table 2 lists the measurements of the observed Hα and Hβ lines for three observing runs. Note also that the ratio of blue-ward flux to red-ward flux is 33:67 (at $\phi = 0.24$) and 35:65 (at $\phi = 0.98$), respectively, whereas their strengths are reversed when the GS is in front, where the ratio of blue-ward and red-ward flux is 59:41 at $\phi = 0.56$. Such a reversal of relative intensities is likely to be caused by the positions of the two components relative to the observer. LH18 confirmed that the Hα and Hβ lines observed in 1998 both formed in the ionized gas (H II) region, with the H atom number density being $\sim 10^{9.8}$ cm^{-3}. LH18 showed that the broad line with a FWHM of 400–500 km s^{-1} is the result of Raman scattering.

As noted for other Balmer profiles by Lee et al. (2017), the Raman scattering mechanism does not play a role in the He II or other H I lines, probably because the corresponding Lyman lines are weak for gas densities of order 10^{10} cm^{-3}. The present study assumes an ionized bipolar cone extending from the WD (as in LH18) and confirms that such a cone geometry accommodates the observed double Gaussian line profiles. To do this, we first need to know whether the GS (or its extended atmosphere) blocks the view toward the receding cone when the former is in front of the WD. We will provide arguments in favor of this scenario from our examination of the double Gaussian line profiles.

3. DOUBLE GAUSSIAN LINE PROFILES FROM THE BIPOLAR CONE

The Raman scattering is probably due to the small distance between the GS atmosphere and the WD. Figure 3 schematically shows the size and relative position of both companions, assuming that AG Peg is a close binary system with both companions on circular orbits. The photons emitted in the ionized region enter into a neutral hydrogen region surrounding the GS where the Raman scattering occurs (Heo & Lee 2015).

As illustrated in Figure 3a, at $\phi \sim 0.25$ the observer (located downward) can observe spectra from both the approaching GS and the receding WD. The spectral

Table 2
Hα and Hβ observed in three epochs

Date	ϕ	Line	Blue	Red	Raman wing	blue:red (%)	mean (%)
1998-09-17	10.24	Hα	1.09(−11)	3.20(−11)	8.15(−11)	25:75	
		Hβ	5.95(−12)	9.07(−12)	3.82(−12)	40:60	33:67
2001-08-30	11.56	Hα	2.29(−11)	1.33(−11)	6.16(−11)	59:41	
		Hβ	7.18(−12)	5.00(−12)	7.53(−13)	59:41	59:41
2002-08-11	11.98	Hα	5.17(−11)	7.99(−11)	1.08(−10)	39:61	
		Hβ	1.43(−11)	3.18(−11)	5.57(−12)	31:69	35:65

Fluxes are in units of $\mathrm{erg^{-1}s^{-1}cm^{-2}}$. Flux values are given in the form 'mantissa(power of ten)'; e.g., 1.03(−11) denotes a flux of 1.03×10^{-11} $\mathrm{erg^{-1}s^{-1}cm^{-2}}$. See LH18 for measurement errors.

data for $\phi = 0.56$ observed in 2001 correspond to the case where the observer is located leftward (in case of counter clock-wise revolution). At phases $\phi \sim 0.0$ or $\phi \sim 0.5$, the stars are aligned with the line of sight. It is not possible to observe the emission line profiles when the GS blocks the view onto the WD and the ionizing gas. However, the observer can see parts of the bipolar conical emission zone whenever the GS cannot block the view onto the ionizing gas completely. We conclude that a semi-detached binary geometry describes the AG Per system better than a close-binary geometry. Figure 4 shows the relative positions of the GS and the WD in a semi-detached binary system. Gas flows from the GS to the WD through the Lagrange point L1, filling some of the WD-side Roche lobe (see Figure 3b). The Roche lobe around the GS is about 20% larger than the GS itself. A strong stellar wind with a terminal velocity of $\sim$1000 $\mathrm{km\,s^{-1}}$ is believed to be produced by the slow nova eruption of the WD beginning in 1850 (Eriksson et al. 2004). Hence, one may assume the presence of a mass-loaded strong stellar wind from the WD, which would push the outer shell gas outward and form a cone-shaped bipolar outflow.

Figure 5 shows a schematic diagram of the bipolar conical outflow, originating from the compact accretion disk around the WD. 'HII' indicates the H II zone ionized by the hot WD star, while 'HI' indicates the neutral zone that surrounds the H II zone. Kenyon et al. (1993) and Eriksson et al. (2004) presumed the presence of a collision region between the WD and the GS where the fast (velocity of $\sim$700 $\mathrm{km\,s^{-1}}$) wind from the WD collides with the wind from the GS (which has a velocity of $\sim$60 $\mathrm{km\,s^{-1}}$), forming composite line profiles with $\sim$200-$\mathrm{km\,s^{-1}}$ doublets. However, LH18 showed that the broad line is actually a Raman scattering line, arising from the high column density of the nearby H I zone. Both H I and H II shells may exist within the conical shell, whose boundary is defined by the outer radius of the inner ionized H II zone where the UV photons from the WD have largely been absorbed. The photoionization (P-I) model by KH08 indicates that the temperature of the WD is about 100 000 K. Such a high WD temperature would produce mass-loaded fast stellar winds. The expanding outflows from the hot WD interact with parts of the CE and push them outwards, forming the expanding ionized bipolar cones with velocities ranging from 50 to 100 $\mathrm{km\,s^{-1}}$.

Figure 6 shows theoretical double Gaussian line profiles calculated for a bipolar conical shell model with the physical parameters given in Table 3. The physical parameters are from Case A of Table 7 by LH18. The bipolar conical shells comprise a H II emission zone, which is responsible for the optical emission lines, surrounded by the outer neutral H I zone. The bipolar conical shell is largely hollow with a thin H II zone whose inner and outer radii are 3.16×10^{13} cm and 3.18×10^{13} cm ($\sim$2.1 au), respectively (see Model I by LH18). Since the bipolar conical shells expand radially outwards from the WD, one can observe the double peak line profiles. Most of the material in the top conical shell recedes from the observer (cf. Figure 5), causing the red-shifted line component. The material in the bottom conical shell approaches the observer, causing the blue-shifted component. The opening angle of the cone, OA, determines the line width. The inclination of the polar axis, i, determines the separation between the line components.

The expansion speed of the bipolar cones pushed by the stellar wind of the hot WD was assumed to be 70 $\mathrm{km\,s^{-1}}$. The opening angle is OA = 74°, and the inclination of the polar axis relative to the observer on Earth is $i = 55°$; these parameter values give a FWHM of 53 $\mathrm{km\,s^{-1}}$, consistent with the observed 44–55 $\mathrm{km\,s^{-1}}$. Although our model assumes that both conical shells are identical, their sizes or opening angles could be different. We smoothed the synthetic profile with a Gaussian kernel of width $\sigma_G = 15$ $\mathrm{km\,s^{-1}}$, narrower than the expected intrinsic line broadening which is $\sim$45 $\mathrm{km\,s^{-1}}$. The conical shell is related to the Roche lobe of the WD or common envelope (CE), which expands along the polar axis of the rotating WD. The radius of the photoionized zone is larger than the radius of the GS or the orbital path, thus the emission zone responsible for the observed emission lines is not obscured by them.

The synthetic double Gaussian profiles in Figure 6b consist of weaker (23%) blue-shifted and stronger (77%) red-shifted components. This asymmetry can be realized physically by different fractions of volume occupied by matter in the two shells, with the lower shell having a smaller fraction than the upper shell. Alternatively, the lower shell might have a smaller opening angle than the upper shell. The bipolar cones expanding in oppo-

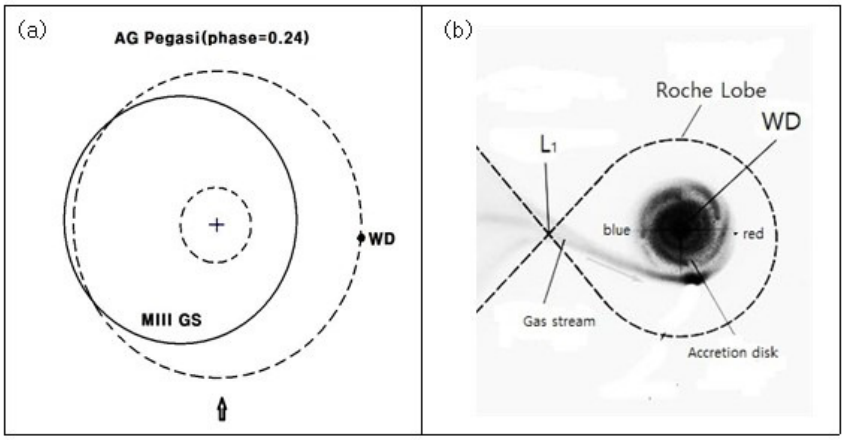

Figure 3. A close binary system viewed face-on. (a) The extended atmosphere of the GS (solid-line circle) arguably corresponds to the Raman scattering zone. Dashed circles indicate orbital paths, the + sign marks the center of mass. The observer (marked by the arrow) is located downward, the orbital phase is $\phi \sim 0.25$. (b) The gas flowing from the GS to the WD through the Lagrange point L1 forms an ionized accretion disk around the hot WD. The dashed line indicates the Roche lobe.

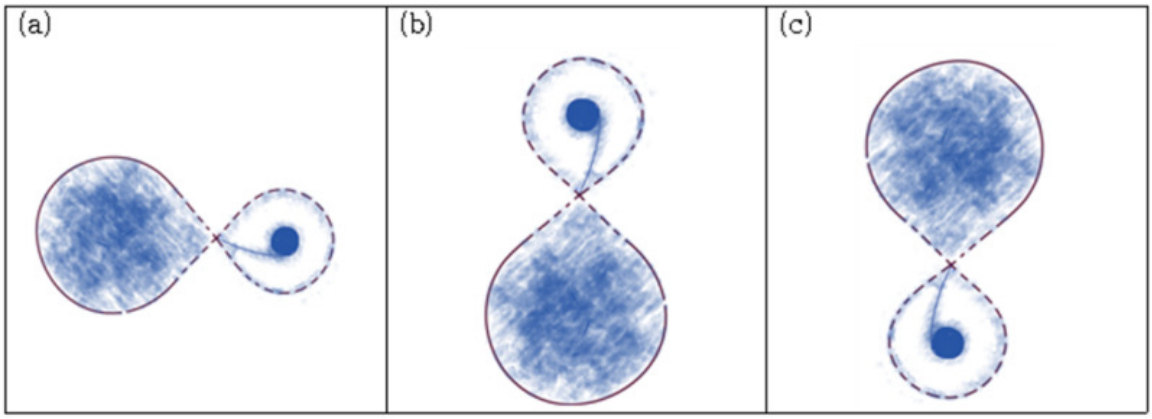

Figure 4. Relative positions of the WD (plus accretion disk) and the GS in a semi-detached binary system at different orbital phases, viewed face-on. The observer is located downward. (a) $\phi \sim 0.25$: Both stars can be observed at the same time. (b) $\phi \sim 0.5$: The WD and the accretion disk are partially obscured, with the degree of obscuration depending on the angle between the line of sight and the orbital plane of the two stars. (c) $\phi \sim 0$: The WD and the accretion disk are observable.

site directions form two peaks, whose separation varies depending on the inclination angle. We found that an inclination $i = 55°$ gives two Gaussian peaks separated by ± 37 km s^{-1}, consistent with our observations. At this stage, we do not yet consider a possible occultation by the GS. The relatively large GS could eclipse some portion of the CE and the conical shell at a specific line of sight.

As seen in Figures 1 and 2, the blue-shifted components of the H I line profiles observed in 1998 were weaker than the red-shifted ones. The ratio of blue-shifted to red-shifted flux intensity, derived from the mean of the Hα and Hβ fluxes, was 33%:67% in 1998 ($\phi \sim 0.25$), which changed to 59%:41% in 2001 (at $\phi \sim 0.5$). The red component became weaker in 2001 (near $\phi \sim 0.5$), suggesting that the extended atmosphere of the GS, or the GS with the CE, obscures the receding portion of the conical shell and the WD itself. However, the red-shifted line component became stronger again in 2002 ($\phi \sim 0.0$). Some earlier studies, e.g., Nussbaumer et al. (1995), Kenyon et al. (1993), and Eriksson et al. (2004), assumed various emission zones located between the GS and the WD to accommodate such a semi-periodic variation. However, such an interpretation is ad hoc and does not provide a self-consistent geometric model. The weaker flux intensities in the blue-shifted lines and the stronger flux intensities in the red-shifted lines appear to be intrinsic, originating from the geometry itself. Hence, the reversal of the flux ratio at $\phi \sim 0.5$ might be due to an eclipse of the emission zone by the extended atmosphere of the GS.

Figure 7 shows the relative positions of the bipolar conical shells and the GS, as well as the accretion disk around the WD, as function of orbital phase (see Figures 3 and 4 for the relative positions of the center of mass and both stars). The H I and H II zones are not specified in this figure, but we assume that the inner radius of the H II zone is comparable to the size of the extended atmosphere of the GS. In Figure 7a, the GS is slightly above the accretion disk plane at phase $\phi = 0.24$, while Figures 7b and 7c show their relative positions at phases 0.56 and 0.98, respectively. At $\phi = 0.24$ and $\phi = 0.98$, the GS does not obscure the conical shell. At $\phi = 0.56$, the GS eclipses parts of the receding (top) conical shell, provided that its atmosphere or the CE are sufficiently extended. Figure 7 assumes that the H II zone is gravitationally bound to the WD. As shown in Figure 2, the kinematic center of the line profiles

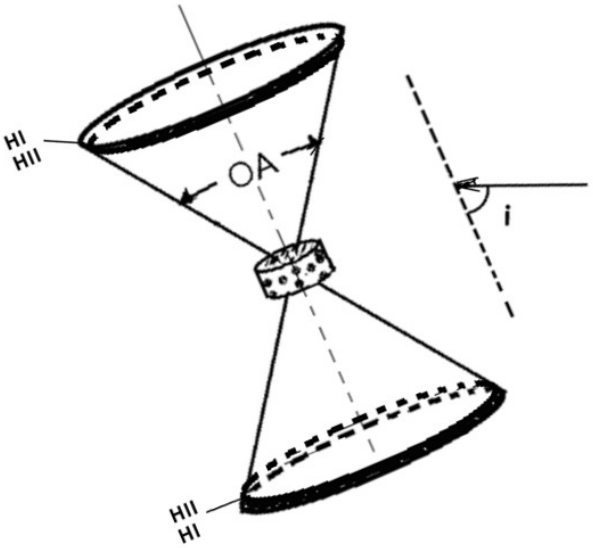

Figure 5. Schematics of the bipolar conical shells and accretion disk around the WD. The bipolar cones are formed by the mass-loaded outflow from the WD against the common envelope. OA: opening angle of the cone; i: inclination angle of the pole relative to the observer located to the right. 'HII' indicates the ionized emission zone in the conical shell, 'HI' indicates the neutral zone.

observed in 1998 is red-shifted by about $+45.0\ \mathrm{km\,s^{-1}}$ compared to the other two years. We did not include the orbital motion into our model.

Figure 8 shows the theoretical line profiles for three phases. Figure 8a shows the line profiles for both $\phi \sim 0.25$ (1998) and $\phi \sim 0.0$ (2002). As discussed above, the blue-shifted line is weaker than the red-shifted one, with a flux ratio of about 35%:65%, indicating that the contribution by the two conical shells is different. Note the position of the GS and the H II conical shell at $\phi = 0.98$ and $\phi = 0.24$ in Figure 7, where the GS does not eclipse the H II region. Figure 8b shows a relatively strong (60%) blue component and a relatively weak (40%) red component (for 2001). Hence, we conclude that the bipolar cone is asymmetric, with a relatively luminous upper cone and a weaker lower cone. The radius of the GS appears to be smaller than the inner radius of the H II zone shell ($R_{\rm i} \sim 2$ au). However, the extended atmosphere (with radius $\mathrm{R_e}$) or the Roche lobe of the GS located between the H II zone and the observer could hide a significant fraction of the H II zone in the upper conical shell due to the relatively large inclination angle, $i = 55°$, because $R_{\rm i} < R_{\rm e} \times (1 + \tan(90° - i))$.

As shown in Figures 1 and 2, the two Gaussian line components are located at $-37\ \mathrm{km\,s^{-1}}$ and $+37\ \mathrm{km\,s^{-1}}$, and accordingly, the predicted peaks have the same separation. We applied a more realistic Gaussian smoothing kernel with a width of $\sigma_{\rm G} = 20\ \mathrm{km\,s^{-1}}$ to the synthetic line profiles in Figure 8. Table 4 summarizes the parameters for the bipolar conical shell model in Figure 7 from which we derive the theoretical line profiles in Figure 8. Note that the parameters in Table 4 are the same as those in Table 3 except of the value of $\sigma_{\rm G}$.

Table 3
Model parameters for 1998 data

Parameter	Value	Unit
$V_{\rm exp}$	70	$\mathrm{km\,s^{-1}}$
Opening angle, OA	74	°
Inclination angle, i	55	°
FWHM	53	$\mathrm{km\,s^{-1}}$
Observed FWHM	44–55	$\mathrm{km\,s^{-1}}$
$\sigma_{\rm G}$	15	$\mathrm{km\,s^{-1}}$

Table 4
Model parameters for 1998, 2001, and 2002 data

Parameter	Value	Unit
$V_{\rm exp}$	70	$\mathrm{km\,s^{-1}}$
Opening angle, OA	74	°
Inclination angle, i	55	°
FWHM	53	$\mathrm{km\,s^{-1}}$
Observed FWHM	44–60 (55)	$\mathrm{km\,s^{-1}}$
$\sigma_{\rm G}$	20	$\mathrm{km\,s^{-1}}$

Figure 9 shows theoretical profiles for (a) the case that both conical shells are of equal luminosity, (b) a different expansion velocity of the shell, and (c) a wide opening angle. As our value of the inclination angle correctly reproduces the observed line separation, we did not vary it. The line profile in Figure 9a corresponds to a phase $\phi \sim 0.35 - 0.40$, while the other two profiles (Figures 9b,c) are calculated at $\phi = 0.56$. Note that a large opening angle not only widens the line profiles but also produces a profile that appears to be composed of three components.

The hot accretion disk may cause an X-ray line with a blue and a red component, which is not discussed in our study. Earlier studies, e.g., Nussbaumer et al. (1995), Kenyon (1986), Kenyon et al. (1993), and Eriksson et al. (2004), identified additional emission: (1) X-ray emission harder than a few 100 eV, possibly emitted by a hot plasma with a temperature of a few million K shock-heated by colliding winds; and (2) a blue-shifted absorption zone from the wind regions and the surrounding nebula, affecting the UV lines and producing P Cygni profiles. The former could be related to the accretion disk or the shock interaction between two stars, while the latter could in part be due to the hot WD and its wind and the cool GS with its extended atmosphere (see also Figures 4 and 7).

4. CONCLUSIONS

Our analysis showed that an expanding bipolar conical shell can explain the observed Hα and Hβ double Gaussian spectral lines, assuming a semi-detached binary system as the most probable structure of AG Peg. The observed H I spectral line profiles are consistent with expanding bipolar conical shells having a polar axis with an inclination angle of $i = 55°$ and an opening angle $\mathrm{OA} = 74°$. The expansion velocity of the shell is prob-

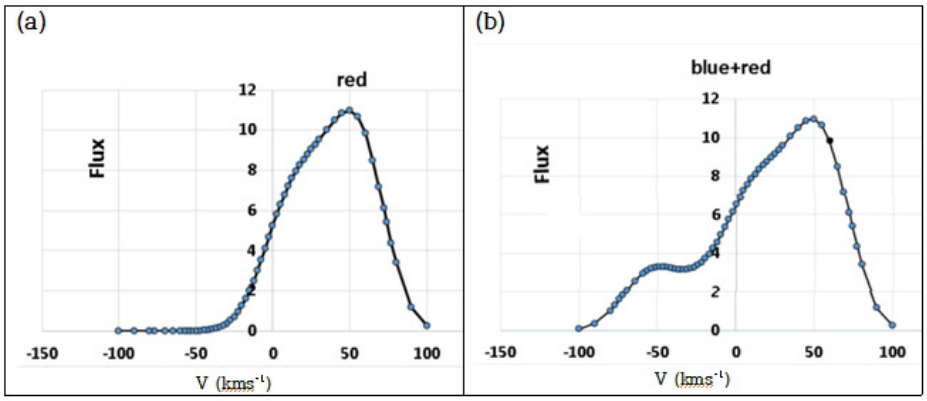

Figure 6. Model line profiles for the spectra obtained in 1998 (at $\phi \sim 0.25$). Fluxes are given in arbitrary units. (a) The red component only (same as Figure 8 in LH18). (b) A synthetic double Gaussian line profile composed of a weaker (23%) blue and a stronger (77%) red component. AG Peg is assumed to be a semi-detached binary system. Note that the center of the broad line in 1998 is red-shifted by about 45 km s^{-1} relative to the 2001 and 2002 centers, which are located at about 0 km s^{-1} (see Figure 2). Hence, the center of the line at $\phi \sim 0.25$ corresponds to $\lambda = 6563.8$ Å for the Hα line and 4862.1 Å for the Hβ line.

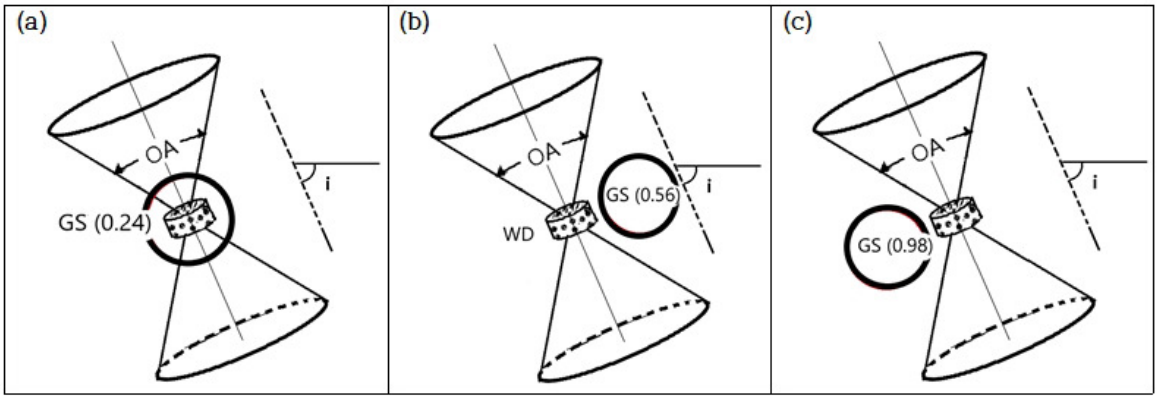

Figure 7. Relative location of bipolar conical shells, the accretion disk around the WD, and the GS (large circle) as function of orbital phase. The observer is located toward the right. (a) At $\phi = 0.24$. (b) At $\phi = 0.56$. (c) At $\phi = 0.98$. At $\phi = 0.24$ and $\phi = 0.98$, the conical shells and the accretion disk are visible to the observer. At $\phi = 0.56$, the extended atmosphere of the GS obscures parts of the receding conical shell. The proposed bipolar cones may be a part of the WD with the common envelope. See also Figure 4 for the relative positions of two stars and the center of mass.

ably about 70 km s^{-1}. The emission zone is probably the result of the interaction of a fast stellar wind from the WD and the gas flowing toward the WD from the GS. The accretion disk around the WD confines the fast stellar wind is confined to a bipolar conical outflow zone. The geometrically thick accretion disk is the highly excited zone responsible for the X-ray emission observed in other studies. As shown by LH18, the Lyman lines can likewise form double Gaussian profiles, which will transform into the broad Balmer Hα and Hβ lines through Raman scattering in the outer H I shell.

Our proposed bipolar conical shells explain the observed double Gaussian profiles (FWHM $\sim$ 60 km s^{-1}), which are also responsible for the broad lines ($\sim$400–500 km s^{-1}) produced by Raman scattering. The upper conical shell appears to differ in size from the lower one. However, when the GS is located between the observer and the WD, the upper conical shell is obscured. The large-scale structure of the expanding gas can be inferred from radio images which indeed show a bipolar shape. Within each cone, the H II zone forms a thin shell which is surrounded by a relatively thick high-density H I shell. KH08 showed that the gas number density of the H II zone is $n_{\rm H} = 10^9 - 10^{10}$ cm^{-3}, while LH18 showed that the outer H I zone has a column density of $N_{\rm H} = 3 - 5 \times 10^{19}$ cm^{-2}. Beyond the outer boundary of the H I zone, there should be a relatively low-density bipolar H I zone on scales of 20″ to 1′, in agreement with 1.5 GHz and 5 GHz radio studies (Kenny et al. 1991).

ACKNOWLEDGMENTS

This research was supported by a grant from the National Research Foundation of Korea (NRF2015 R1D1A3A01019370; NRF2017 R1D1A3B03029309). We are grateful to the late Professor Lawrence H. Aller (UCLA) who joined the HES observation at the Lick Observatory for this study. We express our gratitude

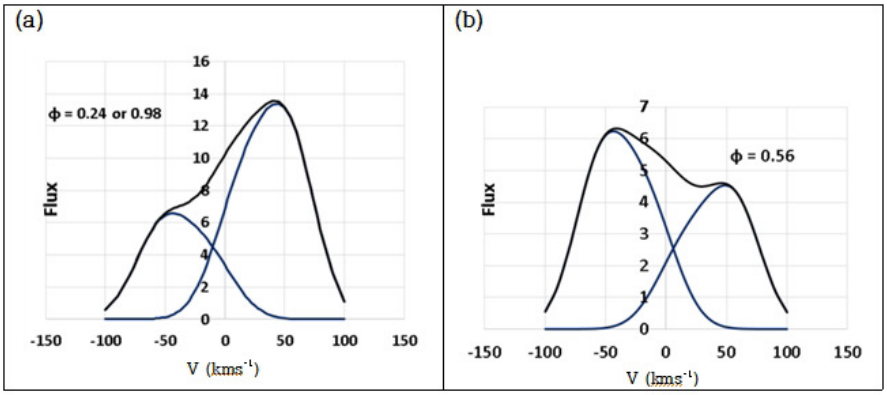

Figure 8. Theoretical line profiles. Flux scales are arbitrary. (a) For $\phi = 0.24$ or $\phi = 0.98$. (b) For $\phi = 0.56$. A velocity of 0 km s^{-1} corresponds to 6562.82 Å for the Hα line and 4861.33 Å for the Hβ line. We did not consider orbital motion. These spectra should be compared to Figures 2 and 6.

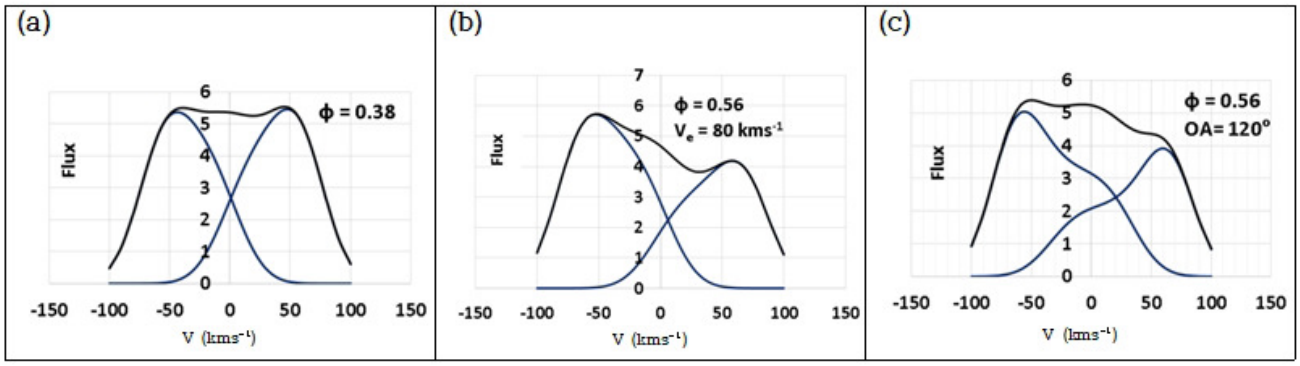

Figure 9. Theoretical line profiles for different values of model parameters. Fluxes are in arbitrary units. (a) For a phase $\phi = 0.35 - 0.40$ when the GS partially obscures the H II zone. (b) For a phase $\phi = 0.56$ and a higher expansion velocity. (c) For $\phi = 0.56$ and a cone opening angle OA = 120°.

to Dr. K.-H. Lee who helped to create Figures 1 and 2. We also thank the anonymous referees for reviewing this paper, and Eugenia H. for proof-reading.

REFERENCES

Allen, D. A. 1980, On the Late-type Components of Slow Novae and Symbiotic Stars, MNRAS, 192, 521

Contini, M. 1997, The Evolving Structure of AG Pegasi, Emerging from the Interpretation of the Emission Spectra at Different Phases, ApJ, 483, 887

Eriksson, M., Johansson, S., & Wahlgren, G. M. 2004, Modeling the Wind Structure of AG Peg by Fitting of C IV and N V Resonance Doublets, A&A, 422, 987

Fleming, W. P. 1907, A Photographic Study of Variable Stars, Ann. Astron. Obs. Harvard College, 47, 1

Heo, J.-U., & Lee, H.-W. 2015, Accretion Flow and Disparate Profiles of Raman Scattered O VI $\lambda\lambda$ 1032, 1038 in the Symbiotic Star V1016 Cygni, JKAS, 48, 105

Hutchings, J. B., Cowley, A. P., & Redman, R. O. 1975, Mass Transfer in the Symbiotic Binary AG Pegasi, ApJ, 201, 404

Kenny, H. T., Taylor, A. R., & Seaquist, E. R. 1991, AG Pegasi: A Multi-shell Radio Source, ApJ, 366, 549

Kenyon, S. J. 1986, The Symbiotic Stars, PhD Dissertation, Harvard University (Boston: Cambridge University Press), 295

Kenyon, S. J., Mikolajewska, J., Mikolajewski, M., et al. 1993, Evolution of the Symbiotic Binary System AG Pegasi: The Slowest Classical Nova Ever Recorded, AJ, 106, 573

Kim, H., & Hyung, S. 2008, Chemical Abundances of the Symbiotic Nova AG Pegasai, JKAS, 41, 23 (KH08)

Lee, H.-W. 2002, Raman-Scattering Wings of Hα in Symbiotic Stars, ApJ, 541, L25

Lee, H.-W., & Hyung, S. 2000, Broad Hα Wing Formation in the Planetary Nebula IC 4997, ApJ, 530, L49

Lee, K. H., Lee, S.-J., & Hyung, S. 2017, An Analysis of the H Emission Line Profiles of the Symbiotic Star AG Peg, JKESS, 2017, 38, 1

Lee, S.-J., & Hyung, S. 2018, The Hα and Hβ Raman-scattering Line Profiles of the Symbiotic Star AG Peg, MNRAS, 475, 5558 (LH18)

Merrill, P. W. 1916, A Spectrum of the P Cygni Type, Pub. Astron. Obs. University of Michigan, 2, 71

Merrill, P. W. 1942, Special Problems of Be Spectra, ApJ, 95, 268

Nussbaumer, H. 1992, The Outburst of Symbiotic Novae, Proc. IAU, 151, 429

Nussbaumer, H., Schmutz, W., & Vogel, M. 1989, Raman Scattering as a Diagnostic Possibility in Astrophysics, A&A, 211, L27

Nussbaumer, H., Schmutz, W., & Vogel, M. 1995, Mass Accretion onto Compact Objects in 2D, A&A, 301, 922

Schmid, H. M. 1989, Identification of the Emission Bands at $\lambda\lambda$ 6830, 7088, A&A, 211, L31

Viotti, R. 1988, The Symbiotic Novae, The Symbiotic Phenomenon Proceedings of the, IAU Coll., 103, 269